Metal Specificity Is Correlated with Two Crucial Active Site Residues in *Escherichia coli* Alkaline Phosphatase[†,‡]

Jie Wang, Kimberly A. Stieglitz, and Evan R. Kantrowitz*

Department of Chemistry, Merkert Chemistry Center, Boston College, Chestnut Hill, Massachusetts 02467

Received January 26, 2005; Revised Manuscript Received March 18, 2005

ABSTRACT: *Escherichia coli* alkaline phosphatase exhibits maximal activity when Zn^{2+} fills the M1 and M2 metal sites and Mg^{2+} fills the M3 metal site. When other metals replace the zinc and magnesium, the catalytic efficiency is reduced by more than 5000-fold. Alkaline phosphatases from organisms such as *Thermotoga maritima* and *Bacillus subtilis* require cobalt for maximal activity and function poorly with zinc and magnesium. Previous studies have shown that the D153H alkaline phosphatase exhibited very little activity in the presence of cobalt, while the K328W and especially the D153H/K328W mutant enzymes can use cobalt for catalysis. To understand the structural basis for the altered metal specificity and the ability of the D153H/K328W enzyme to utilize cobalt for catalysis, we determined the structures of the inactive wild-type *E. coli* enzyme with cobalt (WT_Co) and the structure of the active D153H/K328W enzyme with cobalt (HW_Co). The structural data reveal differences in the metal coordination and in the strength of the interaction with the product phosphate (P_i). Since release of P_i is the slow step in the mechanism at alkaline pH, the enhanced binding of P_i in the WT_Co structure explains the observed decrease in activity, while the weakened binding of P_i in the HW_Co structure explains the observed increase in activity. These alterations in P_i affinity are directly related to alterations in the coordination of the metals in the active site of the enzyme.

Alkaline phosphatase (EC 3.1.3.1) is a nonspecific phosphomonoesterase found in organisms from all kingdoms of life. The mechanism of the alkaline phosphatase reaction involves the attack of a serine alkoxide on the phosphorus of the substrate to form a transient covalent enzyme−phosphate complex followed by the hydrolysis of the serine phosphate (*1*). Alignment of the sequences from a selection of alkaline phosphatases shows that the enzymes are very well conserved, especially near the active site. Upon comparison of residues within 10 Å of the phosphate position in the active site of the *Escherichia coli* enzyme to the corresponding residues in other alkaline phosphatases, the majority of enzymes are found to conserve most of these amino acid positions. The residues that directly interact with the substrate, Ser102 and Arg166, are conserved in all cases. In the *E. coli* enzyme, the active site contains two Zn^{2+} ions and one Mg^{2+} ion. The residues interacting with the zinc at the M1[1] site (Asp327, His331, and His412) and the residues interacting with zinc at the M2 site (Asp51, Asp369, and His370) are conserved in all compared sequences. The only variations occur at amino acids Asp153 and Lys328 near the *E. coli* enzyme Mg^{2+} binding site (M3). Invariably, the only change observed at *E. coli* position 153 is from an Asp to a His. The most common change at *E. coli* alkaline phosphatase position 328 is to a Trp, the exception being a His found in the *Pyrococcus abyssi* and eukaryotic enzymes. In addition to alkaline phosphatases that utilize Zn^{2+} and Mg^{2+}, there are some that utilize cobalt (*2*, *3*). Among the Co^{2+}-requiring enzymes, *Thermotoga maritima* alkaline phosphatase and the *Bacillus subtilis phoAIII* and *phoAIV* gene products have His and Trp at *E. coli* positions 153 and 328, respectively. To test whether positions 153 and 328 alone or in combination determine the metal specificity of alkaline phosphatase, we previously prepared by site-specific mutagenesis the D153H and K328W mutations in the *E. coli* enzyme individually and in combination (*4*).

The wild-type and D153H enzymes showed very little activity in the presence of Co^{2+}. For example, when the Zn^{2+} and Mg^{2+} are replaced with cobalt in the wild-type enzyme, the k_{cat} decreases more than 500-fold (Table 1). However, the k_{cat} of the cobalt-containing K328W enzyme is only ~5-

[†] This work was supported in part by Grant GM42833 from the National Institutes of Health. Data for this study were measured at beamlines X12b and X26c of the National Synchrotron Light Source. Financial support comes principally from the Offices of Biological and Environmental Research and of Basic Energy Sciences of the U.S. Department of Energy, and from the National Center for Research Resources of the National Institutes of Health.

[‡] Coordinates and observed structure factor amplitudes for the structures described in this paper have been deposited in the Protein Data Bank (entries 1Y6V and 1Y7A).

* To whom correspondence should be addressed. E-mail: evan.kantrowitz@bc.edu. Telephone: (617) 552-4558. Fax: (617) 552-2705.

[1] Abbreviations: M1, highest-affinity metal site occupied by Zn^{2+} in the wild-type enzyme; M2, second metal site occupied by Zn^{2+} in the wild-type enzyme; M3, lowest-affinity metal site occupied by Mg^{2+} in the wild-type enzyme; WT_Zn/Mg, wild-type *E. coli* alkaline phosphatase with Zn^{2+} in the M1 and M2 sites and Mg^{2+} in the M3 site (PDB entry 1ED8); WT_Co, wild-type *E. coli* alkaline phosphatase with Co^{2+} in the M1−M3 sites (PDB entry 1Y6V); HW_Co, mutant version of *E. coli* alkaline phosphatase with Asp153 replaced with His and Lys328 replaced with Trp with Co^{2+} in the M1−M3 sites (PDB entry 1Y7A); HH_Zn, mutant version of *E. coli* alkaline phosphatase with Asp153 and Lys328 are replaced with His with Zn^{2+} in the M1−M3 sites (PDB entry 1ANI).

10.1021/bi050155p CCC: $30.25
Published on Web 05/18/2005

Table 1: Kinetic Parameters of the Wild-Type and Mutant Alkaline Phosphatases under Their Optimal Conditions[a]

enzyme	k_{cat} (s^{-1})	K_m (μM)	k_{cat}/K_m (M^{-1} s^{-1})	metal	pH
wild type	167.5 ± 6.0	32.7 ± 5.3	5.1	Zn, Mg	8.0
wild type	0.3 ± 0.5	272 ± 29	0.001	Co	10.0
D153H	47.4 ± 2.7	730 ± 90	0.06	Zn, Mg	10.0
K328W	167.5 ± 15.6	2900 ± 232	0.05	Zn, Mg	10.0
K328W	31.2 ± 4.5	4000 ± 300	0.008	Co, Mg	10.0
D153H/K328W	8.9 ± 0.5	1600 ± 116	0.005	Zn, Mg	10.0
D153H/K328W	43.7 ± 1.3	1940 ± 140	0.02	Co, Mg	10.0

[a] The reactions were performed in 1.0 M Tris-HCl at the indicated pH and 25 °C (*4*). The k_{cat} values were calculated from the V_{max} values obtained by using a dimer molecular mass of 94 000 Da.

fold lower than the k_{cat} of this enzyme in the presence of Zn^{2+} and Mg^{2+}. In the case of the D153H/K328W enzyme, when the Zn^{2+} and Mg^{2+} are replaced with cobalt, the k_{cat} increases ~5-fold (Table 1) (*4*). These studies suggested that the active site residues His and Trp at *E. coli* enzyme positions 153 and 328, respectively, partially dictate the metal specificity of alkaline phosphatase. To understand the structural basis for the altered metal specificity and the ability of the D153H/K328W enzyme to utilize cobalt for catalysis, we determined the structures of the inactive wild-type *E. coli* enzyme with cobalt in the active site, and of the active D153H/K328W enzyme with cobalt in the active site.

EXPERIMENTAL PROCEDURES

Materials

Magnesium chloride, zinc chloride, sodium chloride, cobalt sulfate, sodium dihydrogen phosphate, EDTA, sucrose, and sodium dodecyl sulfate were purchased from Sigma Chemical Co. (St. Louis, MO). Tris and enzyme grade ammonium sulfate were purchased from ICN Biomedicals (Costa Mesa, CA). Phenyl-Sepharose and Source 15Q strong anion-exchange resin were purchased from Amersham Pharmacia Biotech (Piscataway, NJ). Protein Assay Dye and Chelex 100 resin were obtained from Bio-Rad. Crystal cryo-mounting loops were purchased from Hampton Research (Laguna Niguel, CA).

Methods

Expression and Purification of the Wild-Type and D153H/K328W Alkaline Phosphatases. The wild-type and mutant enzymes were isolated from the appropriate pEK548/SM547 plasmid/strain combinations (*4*) by the method described previously (*5*). An additional phenyl-Sepharose column purification step was used for the D153H/K328W enzyme (*4*). The purities of the enzymes were checked by SDS−polyacrylamide gel electrophoresis (*6*). The Bio-Rad version of Bradford's dye-binding assay was used for determination of protein concentrations using the wild-type enzyme as the standard (*7*). Both wild-type and D153H/K328W enzymes were concentrated to approximately 20 mg/mL before use.

Preparation of Wild-Type and Double Mutant Enzymes with Cobalt. The wild-type and D153H/K328W alkaline phosphatases were rendered metal-free using a procedure adapted from Dirnbach et al. (*8*). Five milliliter of 20 mg/mL enzyme was dialyzed against 50 mM Tris and 10 mM EDTA (pH 8.0) to remove extraneous metals and phosphate. Then the enzyme solution was dialyzed twice versus 40% ammonium sulfate and 10 mM EDTA (pH 9.5), followed by extensive dialysis versus 10 mM Tris and 10 mM EDTA (pH 9.0) to remove the ammonium sulfate. The pH was readjusted by another dialysis in 100 mM Tris and 10 mM EDTA (pH 8.0). Finally, the enzyme solution was dialyzed against 100 mM Tris and Chelex (2.5 g/L) (pH 8.0) to remove the EDTA. The enzyme solutions were filtered, and the activity was determined. The lack of enzymatic activity confirmed the absence of metals in the active site (*4*). Cobalt sulfate was then added to the apoenzyme solution to a final concentration of 10 mM.

Crystallization. The wild-type and D153H/K328W cobalt enzymes were dialyzed versus a zinc- and magnesium-free 10 mM cobalt sulfate, 100 mM Tris, 0.85 M $(NH_4)_2SO_4$, 2 mM NaH_2PO_4 (pH 9.5) protein-stabilization buffer, before being concentrated to ~40 mg/mL. Vapor diffusion was used to crystallize each enzyme using 2 μL hanging drops. Within approximately 1 week, crystals of the WT_Co enzyme formed in reservoirs with ammonium sulfate concentrations ranging from 2.0 to 2.2 M. Crystal sizes varied from 0.6 mm × 0.3 mm × 0.3 mm to 0.8 mm × 0.6 mm × 0.3 mm. Crystals of the HW_Co enzyme required ~3 months to form, in reservoirs with the ammonium sulfate concentration ranging from 2.2 to 2.3 M. The size of the crystals formed varied from 0.8 mm × 0.3 mm × 0.3 mm to 2.2 mm × 0.6 mm × 0.3 mm.

Data Collection. Before being mounted, the crystals were transferred into a crystal stabilization buffer composed of 3.0 M $(NH_4)_2SO_4$, 100 mM Tris, 2 mM NaH_2PO_4, and 10 mM $CoSO_4$ (pH 7.5) for at least 24 h. Crystals were transferred to cryo-loops and soaked in a mixture of 80% crystal stabilization buffer and 20% glycerol for ~1 min before being dipped in liquid nitrogen. Data were collected at the National Synchrotron Light Source at Brookhaven National Laboratory (Upton, NY) on beamlines X12b and X26c. Diffraction data were collected to 1.60 and 1.77 Å for the WT_Co and HW_Co crystals, respectively (Table 2). The data sets were processed with HKL2000 (*9*).

Model Building and Structure Refinement. The initial model for the refinement of the WT_Co and HW_Co structures was based on the coordinates of *E. coli* alkaline phosphatase determined to 1.75 Å resolution with all ligands removed from the active sites (PDB entry 1ED8) (*10*). Although the crystals of WT_Co and HW_Co are in the same space group as those of the starting model, there were significant differences (>3 Å) along the *b* and *c* axes. *R* and R_{free} equaled ~28 and 30%, respectively, after the first rigid body and simulated annealing refinement in CNS (*11*). To improve the initial model, automated molecular replacement (AMoRe) was performed on both data sets using a monomer as the starting model to improve the dimer interface and crystal lattice packing.

After model building with AMoRe had been carried out, a round of refinement was performed with CNS. Ten percent of the reflections were not used in the refinement and were used to calculate R_{free}. The metals, phosphate, and sulfate were introduced into both structures. After each refinement cycle, visual inspection and manual rebuilding were performed in XtalView (*12*) to improve the working *R* and R_{free} values. The final stages of the refinement were performed using SHELX-97 (*13*). After the first round of refinement

Table 2: Data Collection and Refinement Summary of the WT_Co and HW_Co Structures

	WT_Co	HW_Co
data collection		
space group	*I*222	*I*222
resolution (Å)[a]	30−1.60 (1.66−1.60)	30−1.77 (1.83−1.77)
total no. of reflections	1095637	1345266
no. of unique reflections	160264	111560
redundancy[a]	6.9 (6.5)	12.0 (10.3)
completeness (%)[a]	99.5	94.6 (89.6)
unit cell (Å)	$a = 76.475$	$a = 76.208$
	$b = 164.257$	$b = 164.564$
	$c = 192.819$	$c = 192.636$
angles (deg)	$\alpha = \beta = \gamma = 90$	$\alpha = \beta = \gamma = 90$
R_{merge} (%)[a,b]	5.3 (28.8)	8.5 (23.9)
refinement		
resolution (Å)	30−1.60	30−1.77
average I/σ	14.9	26.6
R	0.191	0.205
R_{free}	0.212	0.238
no. of waters	714	670
average B factor (Å^2)	25.83	28.86
rms deviations		
bonds (Å)	0.0196	0.0248
angles (deg)	1.95	2.17
dihedrals (deg)	24.42	24.36

[a] Data in parentheses correspond to the highest-resolution shell. [b] $R_{merge} = \Sigma(I_{hkl} - I_{\overline{hkl}})/\Sigma I_{\overline{hkl}}$, where I_{hkl} is the observed intensity and $I_{\overline{hkl}}$ is the mean intensity of the observed intensity.

in SHELX-97, waters were added. The models were returned to CNS for final *B* factor refinement. The mobility of active site metals and phosphate was evaluated by inspecting the $F_o - F_c$ electron density map for alternate positions and by occupancy refinement in CNS. The final R and R_{free} values as well as the refinement statistics are reported in Table 2.

RESULTS

Structures of the Wild-Type and D153H/K328W Cobalt Enzymes. The data for wild-type AP with cobalt (WT_Co) and the D153H/K328W enzyme with cobalt (HW_Co) were integrated, scaled, and averaged to space group *I*222, the same space group that was observed for the wild-type structure with zinc and magnesium (WT_Zn/Mg) (PDB entry 1ED8) (*10*). The WT_Co and HW_Co structures were refined to R values of 19.1 and 20.5% and R_{free} values of 21.2 and 23.8% at resolutions of 1.60 and 1.77 Å, respectively. The unit cell dimensions, data collection statistics, and refinement statistics are given in Table 2.

The electron density in the active site region of the WT_Co structure is shown in Figure 1A. When the $2F_o - F_c$ electron density map is contoured at 2.0σ or lower, electron density completely covers every residue in the active site, indicating the active site is well-refined. The position of the side chain of Lys328 is stabilized by interactions with Asp327 and Asp153. Lys328 forms a water-mediated interaction with Asp327 and a salt link with Asp153. There is also a water-mediated interaction between Asp153 and Arg166. Inorganic phosphate (P_i), the product of the reaction, is positioned in the active site pocket via three coordination bonds to the cobalt ions in the M1 and M2 sites. Two phosphate oxygens also interact in a bidentate fashion with the terminal nitrogens of Arg166. The average *B* factor for the side chain of Arg166 is 18.87 Å^2, and the *B* factor for the P_i is 24.71 Å^2 at 100% occupancy (Table 3).

The electron density in the active site of the HW_Co structure is shown in Figure 1B. The positions of the two mutant residues, His153 and Trp328, were confirmed by evaluation of simulated annealing omit maps produced with CNS (*11*). Trp328 is repositioned toward the solvent and away from the active site. His153 coordinates directly to the cobalt ion in the M3 site. The *B* factors for the Trp328 and His153 side chains were 49.88 and 27.64 Å^2, respectively. The coordination of His153 to the cobalt ion prevents His153 from forming a water-mediated interaction with Arg166, which does occur in the wild-type structure. In this structure, Arg166 interacts in a bidendate fashion with a water molecule and is involved in binding P_i. The average *B* factor of the Arg166 side chain is 33.24 Å^2, while the average *B* factor for the P_i is 70.84 Å^2 with an occupancy of 60% (Table 3).

Geometry of the Three Metals in the Active Site of the WT_Co Structure. In the WT_Co structure, each active site has three cobalt ions bound in positions very similar to those observed for the zinc and magnesium ions in the WT_Zn/Mg structure. A summary of the interactions involving the three cobalt ions in the WT_Co structure as well as the corresponding distances and angles can be found in Tables 4 and 5, respectively.

The cobalt in the M1 site is coordinated to Asp327, His331, His412, and P_i, and adopts approximate octahedral geometry (see Figure 2). $His412^{NE2}$, $Asp327^{OD1}$, $Asp327^{OD2}$, and P_i^{O2} are coplanar, each interacting with the cobalt at distances between 2.02 and 2.42 Å. These interactions are confirmed by the presence of electron density at 2.0σ (see Figure 2 and Table 4). The angles between the two bonding atoms and the cobalt are all close to 90° except in the case of the $Asp327^{OD1}$−Co−$Asp327^{OD2}$ angle, which is 57.8° due to the restraints imposed by the carboxyl group of Asp327 (Table 5). The requirement to keep the two oxygen atoms of Asp327 close together prevents these oxygen atoms from forming optimal coordination with the cobalt. The apical $His331^{NE2}$−Co−apical PO_4^{O3} angle of 169.4°, which is close to 180°, also supports an octahedral geometry for the cobalt at the M1 site.

The cobalt ion in the M2 site adopts a trigonal bipyramidal geometry (see Figure 2). $Ser102^{OG}$, $His370^{NE2}$, $Asp369^{OD1}$, and the cobalt are in the same plane, and the angles between the two bonding atoms and the cobalt in the equatorial plane are 131.5°, 113.5°, and 115.1°, all reasonably close to the expected value of 120°. The apical P_i^{O3}−Co−apical $Asp369^{OD1}$ angle of 156.7° deviates slightly from the ideal value of 180°. However, this distortion may be due to the backbone restraints the enzyme imposes upon residues in the active site.

The cobalt ion in the M3 site also adopts an octahedral geometry. Three water ligands to the cobalt offer lower constraints, making it much easier for this cobalt to attain perfect octahedral geometry. The coordinate bond distances range from 1.91 to 2.15 Å, and the angles between these bonds range from 83.3° to 98.1°, all falling within the ideal coordination bond distance or angle range (see Figure 2).

Geometry of the Three Metals in the Active Site of the HW_Co Structure. The geometries of cobalt at the M1 and M2 sites in the HW_Co structure are the same as those in the WT_Co structure: octahedral and trigonal bipyramidal, based on the observed bond distances and angles (see Figure 2).

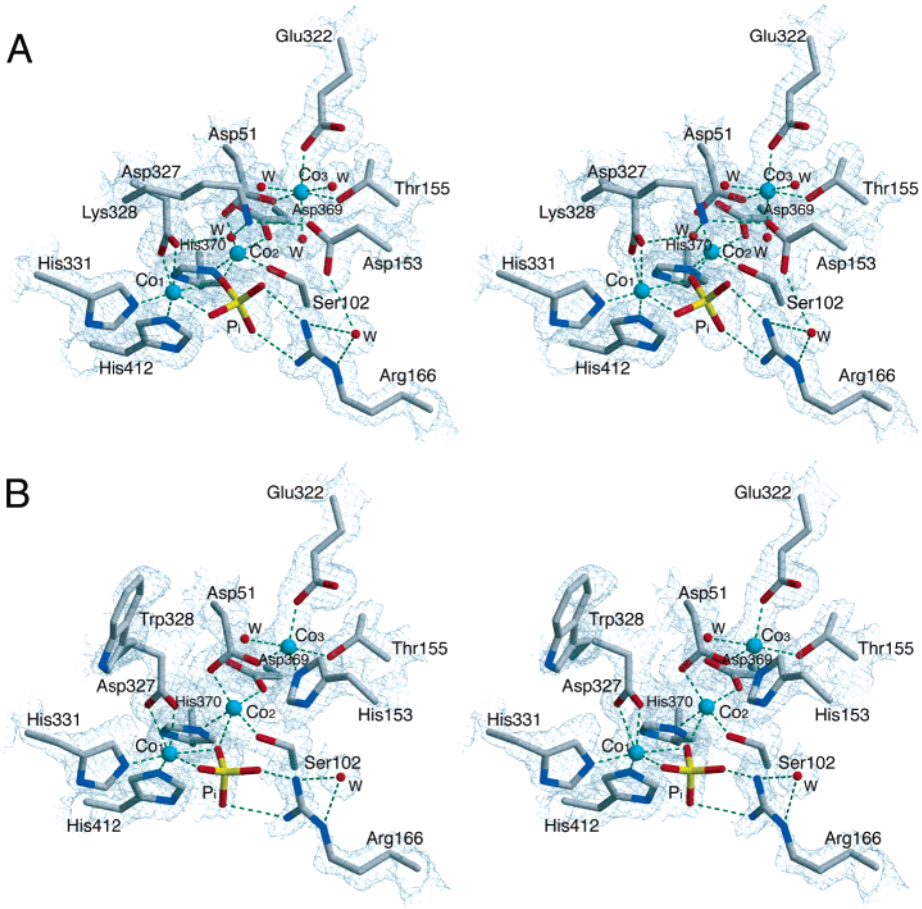

FIGURE 1: Stereoview of the active site of the WT_Co and HW_Co structures. Shown are the $2F_o - F_c$ electron density maps for (A) WT_Co (2.0σ) and (B) HW_Co (1.2σ, to show the density of the Arg166 and the P_i). Overlaid on the electron density are the final refined coordinates. Water molecules are shown as red spheres and Co atoms as larger cyan spheres. Dashed lines represent hydrogen bonds. Figures 1−5 were prepared using MOLSCRIPT (*24*).

Table 3: Occupancy and *B* Factors of Some Ligands and Active Site Residues in the WT_Zn/Mg, WT_Co, HH_Zn, and HW_Co Structures

	B factor (Å^2)[a]			
residue	WT_Zn/Mg	WT_Co	HH_Zn	HW_Co
Ser102		21.10	7.45	27.10
Arg166	18.06	18.87	49.25	33.24
Asp/His153	19.03	19.28	7.92	27.64
Lys/His/Trp328	17.40	19.06	64.99	49.88
P_i[b]	1.00/20.67	1.00/24.71	0.69/76.94	0.60/70.84

[a] The values reported are the average *B* factors of the side chains of the A and B chains. [b] Reported are the occupancy and *B* factor of the P_i averaged over the A and B chains.

For the cobalt in the M3 site, the side chain of His153 becomes a direct ligand and replaces two of the water molecules that coordinate to the M3 cobalt in the WT_Co structure. Asp51^{OD1}, Glu322^{OE2}, His153^{ND1}, and this cobalt are almost coplanar, with equatorial angles ranging from 110.4° to 125.3° (Table 4). In addition, the Glu322^{OE2}−Co−Asp51^{OD1} angle is shifted from 98.1° in the WT_Co structure to 110.4° in HW_Co structure. Take together, these observed angles suggest that the geometry of cobalt at the M3 site has changed from octahedral in the WT_Co structure to trigonal bipyramidal in the HW_Co structure (see Figure 2).

Active Site Comparison of the WT_Co and WT_Zn/Mg Structures. Comparison of the WT_Co and WT_Zn/Mg structures after a least-squares fit of the coordinates revealed two major differences between the structures in the active site region. First, there is an alteration in the position of the Ser102 side chain and, second, a change in the position of the P_i. In the WT_Co structure, there is only one conformation for the side chain of Ser102, in which Ser102^{OG} forms a very strong coordinate bond with the M2 cobalt. In contrast, there are two conformations of the side chain of Ser102 with occupancies of approximately 40 and 60% in the WT_Zn/Mg structure (PDB entry 1ED8): the predominant conformation has the hydroxyl of Ser102 coordinated to zinc, whereas in the alternative conformation, this hydroxyl forms a hydrogen bond with Thr155 (see Figure 3). In the WT_Co structure, the interaction between Ser102^{OG} and the M2 cobalt is very strong, as judged by the persistence of the electron density to 4.0σ. This strong coordinate bond would prevent the hydroxyl group from rotating to attack the substrate, which is consistent with the observed decreased k_{cat} value of the WT_Co enzyme compared with that of the the WT_Zn/Mg enzyme (*4*).

The second major difference between the WT_Co and WT_Zn/Mg structures is the precise coordination of the P_i. In the WT_Co structure, the P_i is shifted 0.16 Å closer to the M1 cobalt and rotated ~23° so that the distance between P_i^{O3} and this cobalt decreases from 2.87 to 2.34 Å, allowing direct coordination with the cobalt. The three coordinate interactions between the P_i and the cobalt at the M1 and M2

Table 4: Metal−Ligand Distances in the Wild Type with Zinc, the Wild Type with Cobalt, D153H/K328H with Zinc, and D153H/K328W with Cobalt

		distance (Å)			
		WT_Zn/Mg[b]	WT_Co[b,c]	HH_Zn[b]	HW_Co[b,c]
Zn1/Co1[a]	His412 NE2	2.02	2.08	1.99	2.07
	His331 NE2	2.08	2.02	2.10	2.13
	Asp327 OD1	2.13	2.02	2.30	2.46
	Asp327 OD2	2.42	2.42	2.10	2.19
	PO_4 O2	2.04	2.14	−	2.03
	PO_4 O3	2.87	2.34	2.90	2.29
Zn2/Co2[a]	Ser102 OG	−	1.91	2.20	2.12
	Asp51 OD2	2.08	1.94	1.90	2.06
	Asp369 OD1	1.80	2.04	1.96	1.96
	His370 NE2	2.03	1.97	2.00	2.20
	PO_4 O3	2.10	1.98	−	2.60
Zn3(Mg3)/Co3[a]	Asp51 OD1	2.02	1.94	1.80	1.99
	Glu322 OE2	2.10	1.91	1.85	1.91
	Thr155 OG1	2.10	2.15	2.20	2.38
	Asp/His153 OD1/NE2	−	−	2.00	1.98
	H_2O	1.98	2.03	−	−
	H_2O	1.95	2.14	−	2.35
	H_2O	2.18	2.09	−	−

[a] The number after the metal refers to the particular metal site in the enzyme (e.g., M1, M2, or M3). [b] WT_Zn/Mg, wild-type with zinc and magnesium (PDB entry 1ED8); HH_Zn, D153H/K328H with zinc (PDB entry 1ANI); WT_Co: wild type with cobalt; HW_Co, D153H/K328W with cobalt. [c] The distances are the average of the distances in A and B chains.

Table 5: Ligand−Metal−Ligand Angles in the WT_Co and HW_Co Structures

		angle (deg)[a]	
		WT_Co	HW_Co
Co1[b]	$His331^{NE2}$−Co−$PO_4{}^{O3}$	169.4	167.5
	$His412^{NE2}$−Co−$PO_4{}^{O2}$	104.3	108.4
	$Asp327^{OD2}$−Co−$PO_4{}^{O2}$	94.6	107.8
	$Asp327^{OD2}$−Co−$Asp327^{OD1}$	57.8	55.9
	$His412^{NE2}$−Co−$Asp327^{OD1}$	98.4	85.5
Co2[b]	$Asp369^{OD1}$−Co−$PO_4{}^{O3}$	156.7	151.3
	$Asp51^{OD2}$−Co−$His370^{NE2}$	113.5	102.5
	$Ser102^{OG}$−Co−$His370^{NE2}$	131.5	122.0
	$Asp51^{OD2}$−Co−$Ser102^{OG}$	115.1	123.4
Co3[b]	$Thr155^{OG1}$−Co−H_2O	180.0	180.0
	$Glu322^{OE2}$−Co−$Asp51^{OD1}$	98.1	110.4
	$Asp51^{OD1}$−Co−H_2O	92.4	
	$Asp322^{OE2}$−Co−H_2O	86.4	
	H_2O−Co−H_2O	83.3	
	$Glu322^{OE2}$−Co−$His153^{NE2}$		125.3
	$Asp51^{OD1}$−Co−$His153^{NE2}$		123.4

[a] The values came from the average of the A chain angles and B chain angles. [b] The number after the metal refers to the particular metal site in the enzyme (e.g., M1, M2, or M3).

sites suggest that the P_i is more tightly bound in the active site of the WT_Co structure than in the WT_Zn/Mg structure.

Comparison of the Active Sites of the WT_Co and HW_Co Structures. Analysis of $2F_o - F_c$, $F_o - F_c$, and simulated annealing omit maps indicated that the HW_Co structure differed significantly from the WT_Co structure locally in the active site region (see Figure 4). The salt link between Asp153 and Lys328, present in the WT_Zn/Mg and WT_Co structures, is absent in the HW_Co structure. In the HW_Co structure, Trp328 is found flipped out of the active site; furthermore, the new position is not well defined, as indicated by a lack of electron density even at a contour level as low as 1.0σ. The side chain of Trp328 has an average *B* factor of 49.88 Å^2. The side chain of His153 coordinates directly with the M3 cobalt, changing the cobalt geometry from octahedral in the WT_Co structure to trigonal bipyramidal in the HW_Co structure.

P_i is loosely bound in the active site pocket of the HW_Co structure, exhibiting an occupancy of 0.60 with a *B* factor of 70.84 Å^2. These values provide an explanation for the reduced affinity of the substrate observed for the HW_Co enzyme as compared to those for the WT_Co and WT_Zn/Mg enzymes (*4*).

Structural Comparison of the Active Site of the HW_Co and HH_Zn Structures. In the structure of the D153H/K328H alkaline phosphatase (HH_Zn, PDB entry 1ANI) (*14*), all the metal sites have zinc present even though the crystal stabilization buffer contained both Zn^{2+} and Mg^{2+}. The D153H mutation resulted in the conversion of the M3 site for a magnesium to a zinc site, as was verified in the structure of the D153H single mutant (PDB entry 2ANH) (*14*).

When the HW_Co and HH_Zn structures were compared after superposition, differences in the position of the P_i and the side chains of some active site residues were observed, as well as the coordination geometry of the metal ions (see Figure 5).

In contrast to its location in the HW_Co structure, in the HH_Zn structure the P_i no longer coordinated to the M1 and M2 metals and has moved 3.0 Å out of the active site toward the solvent. Arg166 is repositioned, losing two coordinate bonds with water molecules, and shows two weak hydrogen bonds to the P_i, indicated by longer hydrogen bond lengths of 3.4 and 2.9 Å. All three zinc ions adopt tetrahedral or distorted tetrahedral geometry based on the metal−ligand distances in the HH_Zn structure (Table 3). In the HW_Co structure, a water molecule coordinates to the M3 cobalt; however, there is no water coordinated to the zinc at the M3 site in the HH_Zn structure. This water molecule switches the geometry of the metal from tetrahedral in the HH_Zn structure to trigonal bipyramidal in the HW_Co structure.

DISCUSSION

The metal specificity of a number of alkaline phosphatases is known. Many require zinc and magnesium; however, some

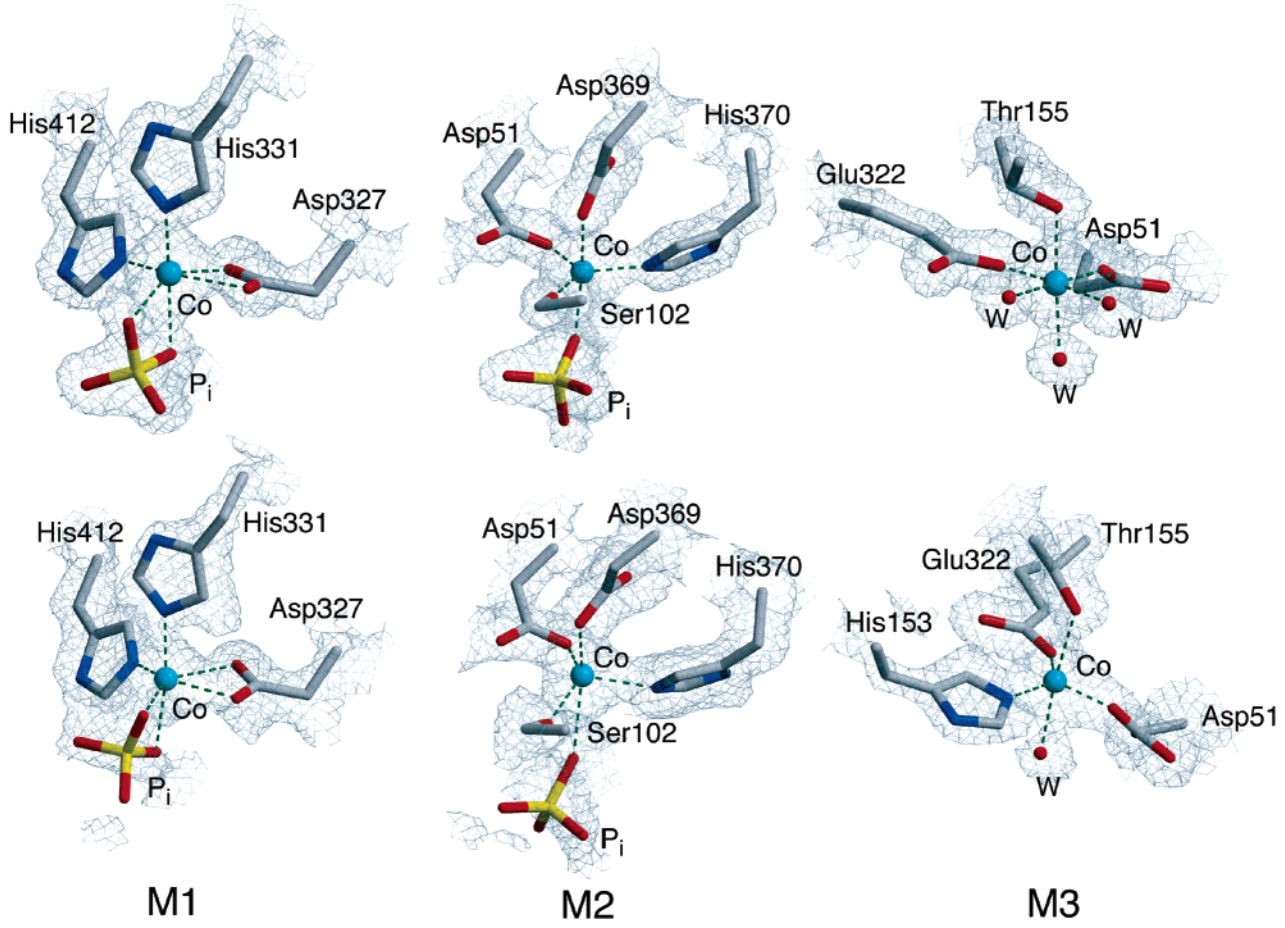

FIGURE 2: Metal geometry of the six cobalt ions in the WT_Co (top) and HW_Co (bottom) structures. Shown are the $2F_o - F_c$ electron density maps contoured at 2.0σ for the WT_Co structure, 1.2σ for the M1 and M2 sites, and 1.5σ for the M3 site for the HW_Co structure. Overlaid on the electron density are the final refined coordinates.

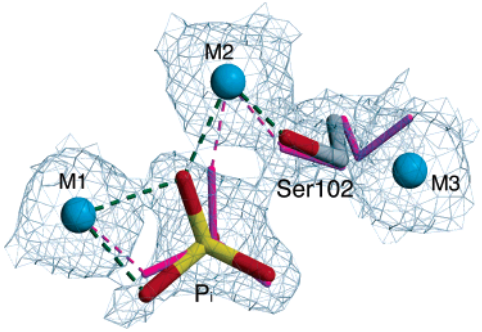

FIGURE 3: Comparison of the position of Ser102 and P_i in the WT_Co and WT_Zn/Mg structures. Shown is the $2F_o - F_c$ electron density map of the WT_Co structure (2.0σ). Overlaid on the electron density are the final refined coordinates of the WT_Co structure (elemental colors, thick lines) and the WT_Zn/Mg structure (*10*) (magenta, thin lines). The ligands with unchanged positions are not shown. In the WT_Co structure, the P_i has three coordinate bonds with cobalt in the M1 and M2 sites, while the Ser102 hydroxyl group coordinates with cobalt in the M2 site. In the WT_Zn/Mg structure, P_i has one coordinate bond to the M1 and M2 zinc ions, while the Ser102 hydroxyl group exhibits two conformations, one coordinated to the zinc ion in the M2 site and the other interacting with a water (hydroxyl) ligand to the Mg^{2+} in the M3 site.

require cobalt (*2*, *3*). A comparison of metal specificities and sequence alignments reveals that enzymes that require zinc and magnesium have Asp at position 153 and Lys at position 328 (*E. coli* numbering), while those that require cobalt have His at position 153 and Trp at position 328. We have previously mutated *E. coli* AP, introducing His and Trp at positions 153 and 328, respectively (*4*). The D153H/K328W cobalt enzyme has a k_{cat} 145-fold higher than that of the cobalt-containing wild-type enzyme. Furthermore, the k_{cat} of the D153H/K328W cobalt enzyme is only ~3-fold lower than the k_{cat} of the Zn- and Mg-containing wild-type enzyme (see Table 1). Here we use X-ray crystallography to determine the structures of the wild-type and D153H/K328W enzymes with cobalt as the metal cofactor to clarify the structural basis of the altered metal specificity of these alkaline phosphatases.

One of the major differences between zinc and cobalt is that the 3d orbital is filled for zinc ($3d^{10}$) and only partially filled for cobalt ($3d^7$). This d orbital difference allows cobalt to form low-spin complexes, while zinc can form only high-spin complexes. Zn(II) is zinc's predominate oxidation state, and it can form high-spin complexes with tetrahedral, trigonal bipyramidal, or octahedral geometries. Co(II) and Co(III) are the predominate oxidation states of cobalt, allowing the formation of high-spin or low-spin complexes. Co(II) can form low-spin trigonal bipyramidal as well as high-spin octahedral geometry, while Co(III) predominately forms low-spin octahedral complexes (*15*).

M1 Metal Binding Site. The M1 site in the WT_Zn/Mg enzyme contains zinc and has a tetragonal pyramidal geometry (*16*). Zn^{2+} interacts with $His331^{NE2}$, $His412^{NE2}$, $Asp327^{OD1}$, $Asp327^{OD2}$, and one oxygen of the P_i. In both the WT_Co and HW_Co structures, the cobalt at the M1

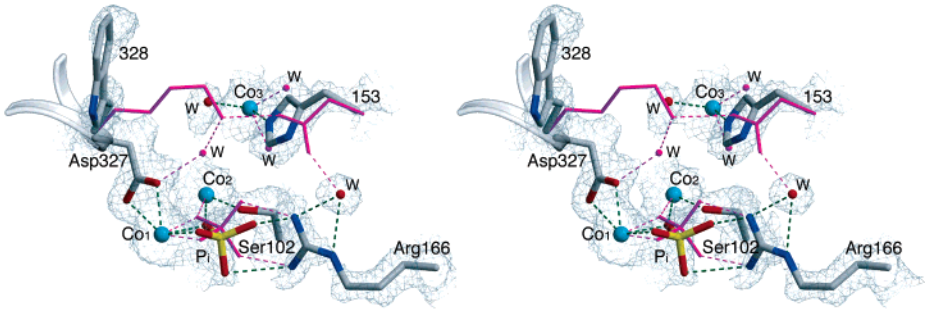

FIGURE 4: Comparison of the coordination of cobalt, water, and P_i in the active sites of the HW_Co (elemental colors, thick lines) and WT_Co (magenta, thin lines) structures. Shown is the $2F_o - F_c$ electron density map of the WT_Co structure (1.2σ). Water molecules are represented as red spheres and cobalt atoms as cyan spheres. The side chains with unchanged positions are not shown.

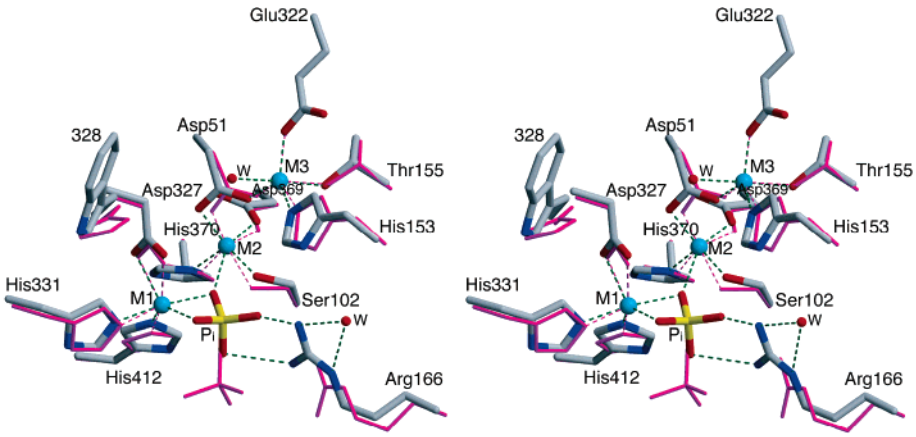

FIGURE 5: Comparison of the active sites of the HW_Co (elemental colors, thick lines) and HH_Zn (*14*) (magenta, thin) structures. Metal positions are represented as cyan spheres, and the water molecule is represented as a red sphere. Dashed lines represent hydrogen bonding interactions.

site has octahedral geometry (see Figure 2). This is consistent with the fact that in known structures of cobalt-containing proteins, the cobalt always adopts octahedral or trigonal bipyramidal geometry independent of the oxidation state (*17*−*19*). The interactions between the cobalt and its ligands are very strong, based upon the observed electron density contour levels in the $2F_o - F_c$ electron density maps. These strong interactions are consistent with low-spin Co(III), but the bond lengths are similar to that observed in the WT_Zn/Mg enzyme, suggesting high-spin Co(II).

M2 Metal Binding Site. The M2 site in the WT_Zn/Mg enzyme contains zinc and has a distorted tetrahedral geometry. Zn^{2+} interacts with His370^{NE2}, Asp51^{OD1}, Asp369^{OD1}, and one oxygen of P_i (*16*). In contrast to the WT_Zn/Mg structure, the cobalt at the M2 site is observed to have trigonal bipyramidal geometry in both the WT_Co and HW_Co structures (see Figure 2).

M3 Metal Site. The M3 site in the WT_Zn/Mg enzyme contains magnesium and has octahedral geometry. The Mg^{2+} is coordinated to three oxygen atoms from Asp51^{OD2}, Glu322^{OE2}, and Thr155^{OG1} and three oxygen atoms from water molecules (*16*). Two of these waters are held in place by additional hydrogen bonding interactions with the carboxylate of Asp153. In addition, the carboxylate of Asp51 acts as a bridge between the M2 and M3 sites. In the WT_Co structure, the geometry of the cobalt at the M3 site is similar to that of Mg in the WT_Zn/Mg structure. However, in the HW_Co structure, the coordination at this site changes from octahedral to trigonal bipyramidal (see Figure 2). In the WT_Co structure, there is sufficient space for three water molecules to approach the cobalt, allowing the cobalt to adopt octahedral geometry. In contrast, in the HW_Co structure, His153^{NE2} forms a coordinate bond to the cobalt, taking the space of two of the three water molecules that interact with the Mg^{2+} in the WT_Zn/Mg structure (see Figure 4). The loss of one coordinating ligand makes it energetically unfavorable for the cobalt to maintain octahedral geometry, so it adopts dsp^3 hybridization and trigonal bipyramidal geometry. The trigonal bipyramidal geometry is verified by the expansion of the Glu322^{OE2}−Co−Asp51^{OD1} angle from 98.1° to 110.4°, and the other two equatorial angles of 123.4° and 125.3° (Table 4).

Co^{2+} versus Zn^{2+}. In the HH_Zn structure, all three metal sites are occupied by zinc (*14*). The zinc at the M3 site adopts tetrahedral geometry with Asp51^{OD2}, Thr155^{OG1}, Glu322^{OE2}, and His153^{NE2} as ligands. In the HW_Co structure, the cobalt at the M3 site adopts trigonal bipyramidal geometry. This observation is consistent with the fact that zinc prefers tetrahedral over trigonal bipyramidal geometry.

WT_Co versus WT_Zn/Mg Structures. Although the metal present in the three metal binding sites is the only difference between the WT_Co and WT_Zn/Mg enzymes, these two enzymes exhibit entirely different catalytic activities. The wild-type enzyme in the presence of Zn^{2+} and Mg^{2+} has a 5000-fold higher catalytic efficiency than the wild-type enzyme in the presence of cobalt at basic pH (see Table 1) (*4*). The cobalt ions in the active site coordinate with P_i as well as with Ser102^{OG} to satisfy their tendency to form an octahedral/trigonal bipyramidal geometry. For the wild-type enzyme with zinc and magnesium, it is known that the release

of the P_i from the noncovalent E·P_i complex is the rate-determining step at basic pH (*20*, *21*). In the case of the WT_Co enzyme, the three coordination bonds between the cobalt and P_i enhance phosphate affinity, impeding the rate-determining step (see Figure 3). Additional rate reduction can also be explained by the strong coordination between the cobalt at the M2 site and $Ser102^{OG}$, which would retard the attack of the serine hydroxyl on the phosphorus of the substrate.

The HW_Co Enzyme Has a Higher Activity than the WT_Co Enzyme. For the wild-type enzyme, it is proposed that Asp153 helps position the side chain of Arg166, by a water-mediated interaction, to bind P_i (*22*). Since this interaction is absent in the HW_Co structure (see Figure 4), these mutations should increase the flexibility of the Arg166 side chain, which in turn should result in reduced P_i affinity. Higher *B* factors determined for Arg166 in the HW_Co structure support the notion that this side chain has enhanced flexibility, and help explain why the HW_Co enzyme had 20-fold higher catalytic efficiency than the WT_Co enzyme (*4*).

D153H/K328W Alkaline Phosphatase Prefers Cobalt for Activity. Previous kinetic studies have shown that the wild-type enzyme loses almost all catalytic activity when the zinc and magnesium in the active site are changed to cobalt. However, only two mutations (D153H and K328W) are required to convert the wild-type enzyme into an enzyme that can function effectively with cobalt (*4*) (see Table 1). Our studies provide a structural explanation for why the wild-type enzyme exhibits almost no activity when cobalt is the metal cofactor, whereas the HW_Co enzyme is active with cobalt as the metal cofactor.

Stable complexes of cobalt are low-spin with stronger coordination bonds than those in the high-spin complexes formed by zinc ions. These strong interactions hold active site residues tightly and therefore may severely compromise the ability of the Ser102 hydroxyl to function as a nucleophile. The strong interaction between $Ser102^{OG}$ and the cobalt explains the diminished activity in the WT_Co enzyme compared to that in the WT_Zn/Mg enzyme.

Summary. The tighter binding of the P_i as well as the rigid position of $Ser102^{OG}$ in the WT_Co structure causes a slower rate of P_i release, as well as a reduction in the rate of the nucleophilic attack by $Ser102^{OG}$ on the substrate. These changes explain the dramatic decrease in enzymatic activity when zinc and magnesium in the wild-type enzyme are replaced with cobalt. A comparison of the WT_Co with HW_Co structures clarifies the influence of the mutation on metal ion specificity. When Asp153 is mutated to His, His153 directly coordinates to the cobalt in the M3 site, causing a switch of geometry from octahedral in the WT_Co structure to trigonal bipyramidal in the HW_Co structure. Because the carboxylate of Asp51 bridges the M2 and M3 sites, this alteration in coordinate geometry at the M3 site has a ripple effect, resulting in a weaker interaction between $Ser102^{OG}$ and the cobalt at the M2 site as well as a weaker interaction between P_i and the cobalt. Taken together, these alterations result in a substantially higher enzymatic activity in the HW_Co enzyme compared to that in the WT_Co enzyme. Finally, the comparison of HW_Co and HH_Zn structures provides structural details about how different metal ions influence active site coordination. The requirement of at least five coordination sites by cobalt alters the geometry of the M3 site from tetrahedral in the HH_Zn structure to trigonal bipyramidal in the HW_Co structure. This alteration in M3 geometry results in a substantially higher catalytic activity for the HH_Zn enzyme as compared to that of the wild-type enzyme (*23*). Overall, these results provide a structural basis for understanding how metal substitutions in the active site of alkaline phosphatase influence the catalytic activity.

ACKNOWLEDGMENT

We thank Howard Robinson from Brookhaven National Laboratory for data collection and assistance with data processing and R. R. Boulanger for many helpful discussions.

REFERENCES

1. Trentham, D. R., and Gutfreund, H. (1968) The kinetics of the reaction of nitrophenyl phosphate with alkaline phosphatase from *Escherichia coli*, *Biochem. J. 106*, 455−460.
2. Hulett, F. M., Kim, E. E., Bookstein, C., Kapp, N. V., Edward, C. W., and Wyckoff, H. W. (1991) *Bacillus subtilis* alkaline phosphatase III and IV. Cloning, sequencing, and comparisons of deduced amino acid sequence with *Escherichia coli* alkaline phosphatase three-dimensional structure, *J. Biol. Chem. 266*, 1077−1084.
3. Wojciechowski, C. L., Cardia, J. P., and Kantrowitz, E. R. (2002) Alkaline phosphtase from the hyperthermophilic bacterium *Thermotoga maritima* requires cobalt for activity, *Protein Sci. 11*, 903−911.
4. Wojciechowski, C. L., and Kantrowitz, E. R. (2002) Altering of the metal specificity of *Escherichia coli* alkaline phosphatase, *J. Biol. Chem. 277*, 50476−50481.
5. Chaidaroglou, A., Brezinski, J. D., Middleton, S. A., and Kantrowitz, E. R. (1988) Function of arginine in the active site of *Escherichia coli* alkaline phosphatase, *Biochemistry 27*, 8338−8343.
6. Laemmli, U. K. (1970) Cleavage of structural proteins during the assembly of the head of bacteriophage T4, *Nature 227*, 680−685.
7. Bradford, M. M. (1976) A rapid and sensitive method for the quantitation of microgram quantities of protein utilizing the principle of protein-dye binding, *Anal. Biochem. 72*, 248−254.
8. Dirnbach, E., Steel, D. G., and Gafni, A. (2001) Mg^{2+} binding to alkaline phosphatase correlates with slow changes in protein lability, *Biochemistry 40*, 11219−11226.
9. Otwinowski, Z., and Minor, W. (1997) Processing of X-ray diffraction data collected in oscillation mode, *Methods Enzymol. 276*, 307−326.
10. Stec, B., Holtz, K. M., and Kantrowitz, E. R. (2000) A revised mechanism of the alkaline phosphatase reaction involving three metal ions, *J. Mol. Biol. 299*, 1303−1311.
11. Brunger, A. T., Adams, P. D., Clore, G. M., DeLano, W. L., Gros, P., Grosse-Kunstleve, R. W., Jiang, J. S., Kuszewski, J., Nilges, M., Pannu, N. S., Read, R. J., Rice, L. M., Simonson, T., and Warren, G. L. (1998) Crystallography & NMR system: A new software suite for macromolecular structure determination, *Acta Crystallogr. D54*, 905−921.
12. McRee, D. E. (1999) XtalView/Xfit: A versatile program for manipulating atomic coordinates and electron density, *J. Struct. Biol. 125*, 156−165.
13. Sheldrick, G. M., and Schneider, T. R. (1997) High-resolution refinement, *Methods Enzymol. 277*, 319−343.
14. Murphy, J. E., Tibbitts, T. T., and Kantrowitz, E. R. (1995) Mutations at positions 153 and 328 in *Escherichia coli* alkaline phosphatase provide insight towards the structure and function of mammalian and yeast alkaline phosphatases, *J. Mol. Biol. 253*, 604−617.
15. Venkataraman, D., Yuhua, D., Wilson, S. H., Hirsch, K. A., Zhang, P., and Moore, J. S. (1997) A coordinationm geometry table of the d-block elements and their ions, *J. Chem. Educ. 74*, 915−918.

16. Kantrowitz, E. R. (2004) *E. coli* Alkaline Phosphatase, in *Handbook of Metalloproteins* (Messerschmidt, A., Bode, W., and Cygler, M., Eds.) pp 71−82, John Wiley & Sons, Ltd., Chichester, U.K.
17. Lowther, W. T., Orville, A. M., Madden, D. T., Lim, S., Rich, D. H., and Matthews, B. W. (1999) *Escherichia coli* Methionine Aminopeptidase: Implications of Crystallographic Analyses of the Native, Mutant, and Inhibited Enzymes for the Mechanism of Catalysis, *Biochemistry 38*, 7678−7688.
18. Maher, M. J., Ghosh, M., Grunden, A. M., Menon, A. L., Adams, M. W. W., Freeman, H. C., and Guss, J. M. (2004) Structure of the Prolidase from *Pyrococcus furiosus*, *Biochemistry 43*, 2771−2783.
19. Miyanaga, A., Fushinbu, S., Ito, K., and Wakagi, T. (2001) Crystal structure of cobalt-containing nitrile hydratase, *Biochem. Biophys. Res. Commun. 288*, 1169−1174.
20. Bloch, W., and Gorby, M. S. (1980) Catalytic mechanism of *Escherichia coli* alkaline phosphatase: Resolution of three variants of the acyl-enzyme mechanism, *Biochemistry 19*, 5008−5018.
21. Coleman, J. E., and Gettins, P. (1983) Alkaline Phosphatase, Solution Structure, and Mechanism, *Adv. Enzymol. 55*, 351−452.
22. Chen, L., Neidhart, D., Kohlbrenner, W. M., Mandecki, W., Bell, S., Sowadski, J., and Abad-Zapatero, C. (1992) 3-D structure of a mutant (Asp101→Ser) of *E. coli* alkaline phosphatase with higher catalytic activity, *Protein Eng. 5*, 605−610.
23. Murphy, J. E., Xu, X., and Kantrowitz, E. R. (1993) Conversion of a magnesium binding site into a zinc binding site by a single amino acid substitution *Escherichia coli* alkaline phosphatase, *J. Biol. Chem. 268*, 21497−21500.
24. Kraulis, P. J. (1991) MOLSCRIPT: A Program to Produce Both Detailed and Schematic Plots of Protein Structures, *J. Appl. Crystallogr. 24*, 946−950.

BI050155P